17th International Conference on Environmental Degradation of Materials in Nuclear Power Systems – Water Reactors
August 9-12, 2015, Ottawa, Ontario, Canada

# COLD-WORK EFFECTS ON STRESS CORROSION CRACK GROWTH IN ALLOY 690 TUBING AND PLATE MATERIALS

S. M. Bruemmer, M. J. Olszta, N. R. Overman and M. B. Toloczko
Pacific Northwest National Laboratory
Richland, WA 99352 USA

## ABSTRACT

High levels of cold work have been shown to promote intergranular stress corrosion cracking (IGSCC) of alloy 690 materials in simulated PWR primary water environments. Crack growth testing has also indicated a heat-to-heat variability in IGSCC susceptibility and a significant effect of the initial material condition and microstructure. Results are summarized for 12 well-characterized CRDM tubing and plate heats as a function of the degree of cold work along with selected tests evaluating behavior in alloy 690 heat-affected-zone regions. Response measured in 36 crack-growth tests is correlated to the degree of cold work, matrix and grain boundary microstructure, hardness and average misorientation densities measured by electron backscatter diffraction (EBSD). Low propagation rates ($<10^{-8}$ mm/s) are discovered for alloy 690 materials cold worked to reductions less than ~18%. For most material conditions, SCC growth rates increase consistently with the measured hardness and EBSD misorientation densities. However, IGSCC susceptibility is reduced for materials given an initial high-temperature anneal and water quench to alter the grain boundary microstructure before cold working. Cold-work damage mechanisms controlling IGSCC in alloy 690 are discussed.

Keywords: alloy 690, cold work, stress corrosion cracking, PWR primary water, hardness, microstructure, grain boundaries.

## INTRODUCTION

Stress corrosion cracking (SCC) susceptibility of cold-worked alloy 690 plate materials in hydrogenated water environments was first reported by Bettis Laboratory [1,2] approximately 8 years ago. These observations are summarized in Figure 1 and revealed high SCC growth rates above the disposition curve for mill-annealed alloy 600. As a result, many international research organizations [3-20] began research activities to investigate this behavior for alloy 690 materials. The detrimental effects of extensive cold work (e.g., $\geq$20% reduction) were confirmed, although the high SCC propagation rates ($>10^{-7}$ mm/s) at low-to-moderate stress intensities have not been observed. In addition, very limited testing has been performed on well-characterized alloy 690 heats as a function of cold work to low levels. These aspects have made it difficult to determine microstructural issues that promote the onset of intergranular (IG) SCC susceptibility in PWR primary water.

A systematic study is summarized in this paper elucidating cold-work effects on crack-growth behavior of alloy 690 in simulated PWR primary water. New experimental results are combined with previous published data [17-22] to map response for 12 well-characterized alloy 690 control rod drive mechanism (CRDM) tubing and plate heats as a function of cold work level. Detailed characterizations were performed and correlations were made to the matrix and grain boundary microstructure, hardness values and average misorientation densities measured by electron backscatter diffraction (EBSD). In addition, selected results are included for alloy 690 heat affected zones and the influence of initial material condition on SCC propagation rates in cold-worked materials. All of these observations are used to gain insights into mechanisms controlling IGSCC susceptibility for alloy 690 materials.

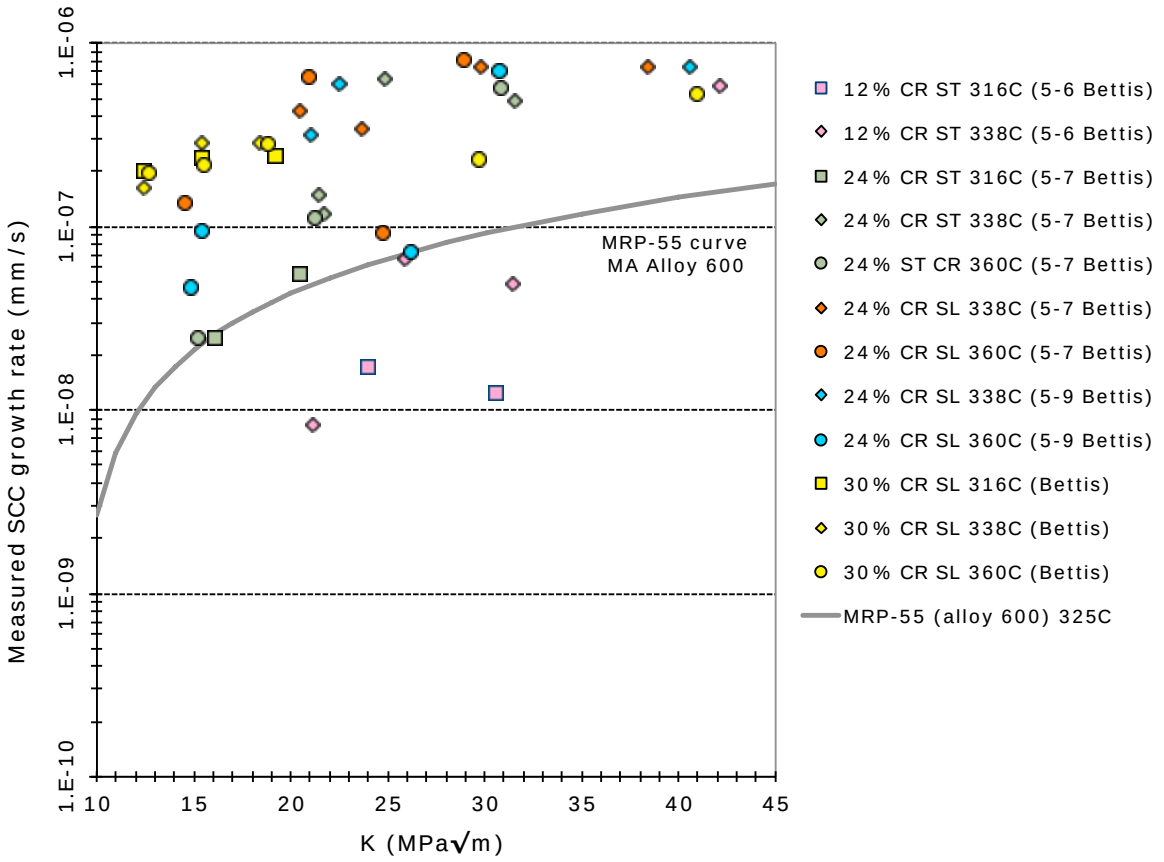


Figure 1. Summary of reported crack-growth-rate measurements in hydrogenated water by Bettis Laboratory [1,2] on cold-worked alloy 690 materials.

## ALLOY 690 MATERIALS AND GENERAL MICROSTRUCTURE

This paper covers testing of 36 crack growth rate specimens representing 12 different heats of alloy 690 in various thermomechanical conditions as shown in Table 1. Most CRDM tubing and bar product forms were tested in the as-received, thermally treated (TT) condition along with plate and billet materials in the mill-annealed (MA) or TT conditions. In addition, the influence of a high-temperature anneal (HTA) before cold working on SCC response was investigated in three heats as well as a recovery heat treatment after cold working. Cold work levels from 0 to 31% were evaluated including measurement of SCC growth rates for one CRDM tubing heat (RE243) in 12 unique thermomechanical conditions.

Detailed microstructural characterizations were conducted on all alloy 690 materials documenting grain structures and second phases in the matrix and at grain boundaries. The density and distribution of IG Cr carbides were of particular interest. Typical examples of the general microstructure and grain boundary precipitation in the CRDM heats are shown in Figure 2(a) and 2(b), respectively. Some differences in grain size can be seen among the as-received TT materials in Table 2, but the morphology and spacing of IG carbides were quite similar. Comparable scanning electron microscopy (SEM) examinations were performed on the plate and billet heats and microstructural observations. Once again, the TT materials exhibited reasonably similar microstructure but the two heats in the MA condition were quite different as described in Table 2. A HTA at 1100°C was given to three heats producing a significant change in microstructure dissolving IG carbide precipitates and an increase in grain size. Grain boundary carbides were completely removed in the CRDM RE243 material leaving only well-spaced TiN particles, while small residual IG carbides remained for the plate heats due to their higher bulk carbon concentrations.

Table 1. Alloy 690 Materials, Material Condition and Average Vickers Hardness

| ID | Source/Producer | Heat # | Form | Condition | Hardness, kg/mm$^2$ |
|---|---|---|---|---|---|
| CT026 | Valinox/Valinox | WP142 | CRDM tube | TT* | 163 |
| CT027 | Valinox/Valinox | WP140 | CRDM tube | TT | 163 |
| CT014 | Valinox/Valinox | RE243 | CRDM tube | TT | 157 |
| CT104 | Valinox/Valinox | RE243 | CRDM tube | TT+11.6%CF$^+$ S-L/S-T | 222 |
| CT020 | Valinox/Valinox | RE243 | CRDM tube | TT+17%CR$^+$ S-L | 249 |
| CT054 | Valinox/Valinox | RE243 | CRDM tube | TT+17%CR S-L | 249 |
| CT100 | Valinox/Valinox | RE243 | CRDM tube | TT+21%CF S-L/S-T | 275 |
| CT022 | Valinox/Valinox | RE243 | CRDM tube | TT+30%CR T-L | 310 |
| CT038 | Valinox/Valinox | RE243 | CRDM tube | TT+31%CR S-L | 315 |
| CT099 | Valinox/Valinox | RE243 | CRDM tube | TT+31%CF S-L/S-T | 302 |
| CT053 | Valinox/Valinox | RE243 | CRDM tube | TT+31%CR S-L+RT$^‡$ | 274 |
| CT015 | Valinox/Valinox | RE243 | CRDM tube | TT+ HTA$^§$ | 155 |
| CT019 | Valinox/Valinox | RE243 | CRDM tube | TT+HTA+17%CR S-L | 251 |
| CT068 | Valinox/Valinox | RE243 | CRDM tube | TT+HTA+17%CR S-L | 251 |
| CT023 | Valinox/Valinox | RE243 | CRDM tube | TT+HTA+30%CR T-L | 312 |
| CT039 | Valinox/Valinox | RE243 | CRDM tube | TT+HTA+31%CR S-L | 316 |
| CT093 | CIEMAT/Valinox | WP787 | CRDM tube | TT+20%TS | 248 |
| CT103 | EPRI/Sumitomo | E67074C | CRDM tube | TT+12.7%CF S-L/S-T | 242 |
| CT098 | EPRI/Sumitomo | E67074C | CRDM tube | TT+31%CF S-L/S-T | 318 |
| CT108 | Doosan/TK-VDM | 133454 | CRDM bar | TT | 156 |
| CT102 | Doosan/TK-VDM | 133454 | CRDM bar | TT+21%CF S-L/S-T | 285 |
| CT084 | ANL/Special Metals | NX3297HK12 | Plate | MA* | 173 |
| CT036 | ANL/Special Metals | NX3297HK12 | Plate | MA+26%CR S-L | 310 |
| CT073 | ANL/Special Metals | NX3297HK12 | Plate | MA+30%CF SL/ST | 316 |
| CT074 | ANL/Special Metals | NX3297HK12 | Plate | HTA+30%CF S-L/S-T | 317 |
| CT085 | GE/Allvac | B25K-2 | Plate | MA | 173 |
| CT037 | GE/Allvac | B25K-2 | Plate | MA+20%CR S-L | 321 |
| CT070 | GE/Allvac | B25K-2 | Plate | HTA+20%CR S-L | 291 |
| CT107 | EPRI/TK-VDM | 114092 | Plate | TT | 165 |
| CT094 | EPRI/TK-VDM | 114092 | Plate | TT+32%CF S-L/S-T | 329 |
| CT060 | ENSA/Aubert&Duval | SP547 | Plate | TT+22%CR S-L | 289 |
| CT059 | ENSA/Aubert&Duval | SP547 | Plate | TT+32%CF S-L/S-T | 305 |
| CT101 | EPRI/Allvac | X87N-1 | Billet | TT+21%CF S-L/S-T | 297 |
| CT067 | ENSA/Aubert&Duval | WP547 | Plate | HAZ | 200-230 |
| CT086 | ANL/Special Metals | NX3297HK12 | Plate | HAZ | 200-240 |
| CT087 | KAPL/Unknown | Unknown | Plate | HAZ | 225-250 |

* As-received condition of the material: Thermally Treated (TT) or Mill Annealed (MA)
$^+$ Cold Forged (CF) or Cold Rolled (CR)
$^‡$ Recovery Treatment (RT): 700°C/1h + Air Cool § High Temperature Anneal (HTA): 1100°C/1h + Water Quench

As summarized in Table 1, nearly all alloy 690 materials were either cold rolled (CR) or cold forged (CF) except for one CRDM heat received from CIEMAT in the tensile strained (TS) condition. This cold work significantly increased the material strength as indicated by the average Vickers hardness. The hardness maps were obtained on cross-section specimens after SCC tests were completed and were taken ahead of the crack front in the crack-growth plane. Details on the hardness testing approach have been described in a previous paper [21]. In general, hardness values increased from ~160 kg/mm$^2$ for the as-received alloy 690 materials to >300 kg/mm$^2$ after ~30% cold work. Some heat-to-heat variability can be seen among materials with an intermediate level of cold work, i.e., near 20%. Three alloy 690 heat affected zone (HAZ) specimens were also evaluated and showed slightly higher hardness values (~20%) close to the weld fusion line.

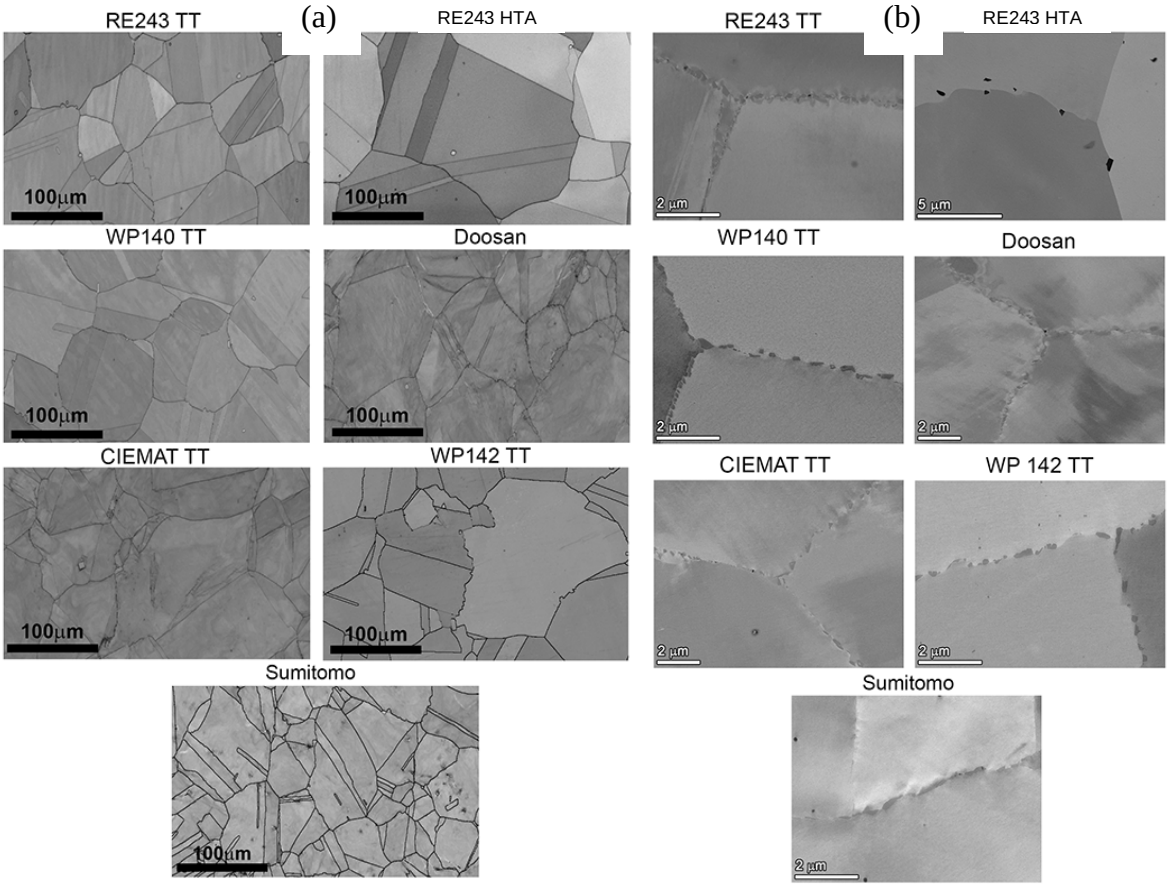


Figure 2. Microstructures images is the six different heats of alloy 690 CRDM material: (a) SEM EBSD pattern quality maps illustrating grain size and (b) SEM BSE images showing typical grain boundary precipitate distributions with materials showing IG Cr carbides except from the RE243 given the HTA where only isolated Ti nitrides are present.

SEM and selected transmission electron microscopy (TEM) examinations have also been conducted on the cold-worked materials. The increase in hardness with cold work results from its effect on the matrix strain and dislocation density. EBSD-measurements of local misorientation effectively document this relationship and a direct correlation between hardness and the integrated misorientation density (IMD) has been established for these alloy 690 materials [22]. Beyond matrix strengthening, high levels of cold work can produce "permanent" damage at grain boundaries in the form of small voids and cracked second phase precipitates (carbides and nitrides). High-resolution SEM backscatter electron (BSE) imaging under low kV conditions proved to be the most effective for sampling a large number of boundaries and identifying fine IG voids and cracks. The most extensive CW-induced damage was found in the ANL Alloy 690MA material in either the 26%CR or 30%CF condition. A high density of voids and a moderate density of cracked carbides were present along grain boundaries, while larger TiN particles in the matrix were also extensively cracked. In comparison, the CRDM and plate materials in the TT starting condition exhibited a moderate density of IG voids and a low density of cracked carbides after cold-work reduction of 30-32%. All of these materials have a semi-continuous distribution of grain boundary carbides, however the ANL MA heat carbides were larger and more in shape than IG carbides in the TT materials. Consistent with the limited number of carbides in the HTA materials, IG voids or cracked carbides were only found in isolated boundary sections. In summary, permanent damage at grain boundaries scaled with the distribution of larger IG carbides. A detailed description of grain boundary damage microstructures is presented elsewhere [23] for all cold-worked alloy 690 materials listed in Table 1.

Table 2. Summary of Grain Size and Carbide Distributions for Selected Materials

| Material | Grain Size (μm) | Carbide Location and Size | Carbide Density and Spacing |
|---|---|---|---|
| **CRDM Materials** | | | |
| Valinox RE243 TT | ~50 | IG, 50-200 nm | Semi-continuous, spacing ~100 nm |
| Valinox RE243 TT+HTA | ~110 | No carbides | No carbides |
| Valinox WP140 TT | ~75 | IG, 50-300 nm | Semi-continuous, spacing ~100 nm |
| CIEMAT Valinox WP787 TT | ~60 | IG, 50-200 nm | Semi-continuous, spacing ~100 nm |
| Valinox WP142 TT | ~60 | IG, 50-300 nm | Semi-continuous, spacing ~100 nm |
| Sumitomo E67074C TT | ~40 | IG, 50-300 nm | Semi-continuous, spacing ~100 nm |
| Doosan TK-VDM 133454 TT | ~60 | IG, 50-200 nm | Semi-continuous, spacing ~100 nm |
| **Plate Materials** | | | |
| GEG B25K MA | ~15 | TG and isolated IG, 0.5-1 μm | Low, sporadic distribution |
| GEG B25K MA+HTA | ~50 | Isolated IG, 20-30 nm | Low, sporadic distribution |
| ANL HK3297HK12 MA | ~25 | IG, 0.3-1.0 μm | Semi-continuous Spacing ~100 nm |
| ANL HK3297HK12 MA + HTA | ~35 | Isolated IG, 10 nm - 1.0 μm | Low, sporadic distribution |
| Allvac X87N-1 TT | ~25 | IG, 50-200 nm | Semi-continuous Spacing ~200 nm |
| TK-VDM 114092 TT | ~40 | IG, 50-200 nm | Semi-continuous Spacing ~200 nm |
| ENSA WP547 TT | ~60 | IG, 50-200 nm | Semi-continuous Spacing ~200 nm |

## STRESS CORROSION CRACK GROWTH RESPONSE AS A FUNCTION OF COLD WORK

Most SCC results summarized in this paper were obtained from tests at 360°C in simulated PWR primary water with 1000 ppm of boron and 2 ppm of lithium. Dissolved hydrogen concentration was 25 cc/kg to fix the corrosion potential at the Ni/NiO line. Crack-growth testing was conducted on 0.5T compact tension (CT) specimens of the various CW Alloy 690 materials in the S-L orientation (CR materials) or S-L/S-T (CF materials). Experiments were routinely performed on two specimens tested in series with K controlled by the specimen showing faster propagation rates. The standard K value used for testing was 30 MPa$\sqrt{m}$, however SCC growth rates were determined at several K levels for most experiments.

Specimens were first fatigue precracked in air followed by extending the precrack by cycling in the high-temperature water environment. A variety of loading conditions were used to transition the TG crack front created in fatigue to an IGSCC crack. Crack growth response was monitored in situ by direct current potential drop (DCPD) with reported propagation rates corrected by post-test measurements on the crack-growth surface. General performance aspects of the crack growth test systems [15,16] and detailed descriptions of the alloy 690 SCC response [16-18,23] have been reported previously.

**As-Received Alloy 690 Materials**

Crack growth testing has been conducted on six as-received alloy 690 materials, four CRDM heats in the TT condition and two plate heats in the MA condition. Most tests were conducted in 360°C PWR primary water, however a few were at 325 or 350°C. K levels were varied from 30 to 40 MPa√m. The typical experimental approach is illustrated in Figure 3 for the GE alloy 690 MA specimen CT085 with three constant K SCC evaluations following extensive transitioning steps. This specimen exhibited the highest measured SCC growth rates among the as-received alloy 690 materials and was the only one where local IG cracking could be resolved. The SCC growth response for these specimens often decreased with time during constant K loading as shown in Figure 4. An initial propagation rate of 1-2x$10^{-9}$ mm/s at constant K was seen for several materials, but would often decay to rates <5x$10^{-10}$ mm/s (essentially no growth) over the first 100-200 hours. The SCC rates reported reflect the stable growth rates after extended exposure at constant K. Data for all as-received alloy 690 materials is plotted in Figure 5 along with measurements on the RE243 heat in the HTA condition (specimen CT015) and three HAZ specimens (CT067, CT086 and CT087). Specific information of these specimens was given in Table 1. Slightly higher growth rates were observed for one of the HAZ specimens as documented in Figure 6, however its maximum stable SCC rate was still <2x$10^{-9}$ mm/s. Crack path (mainly TG) and approximate locations for reported alloy 690 HAZ SCC growth rates for the CIEMAT specimen CT067 in Figure 6 are identified in Figure 7. Microhardness across this region of the HAZ did reveal slightly higher values (~220 kg/mm$^2$) versus the bulk alloy 690 (~200 kg/mm$^2$). The conclusion from tests on alloy 690 materials without cold work is that they are extremely resistant to IGSCC growth under primary water conditions with expected SCC growth rates <2x$10^{-9}$ mm/s and not an issue for PWR service.

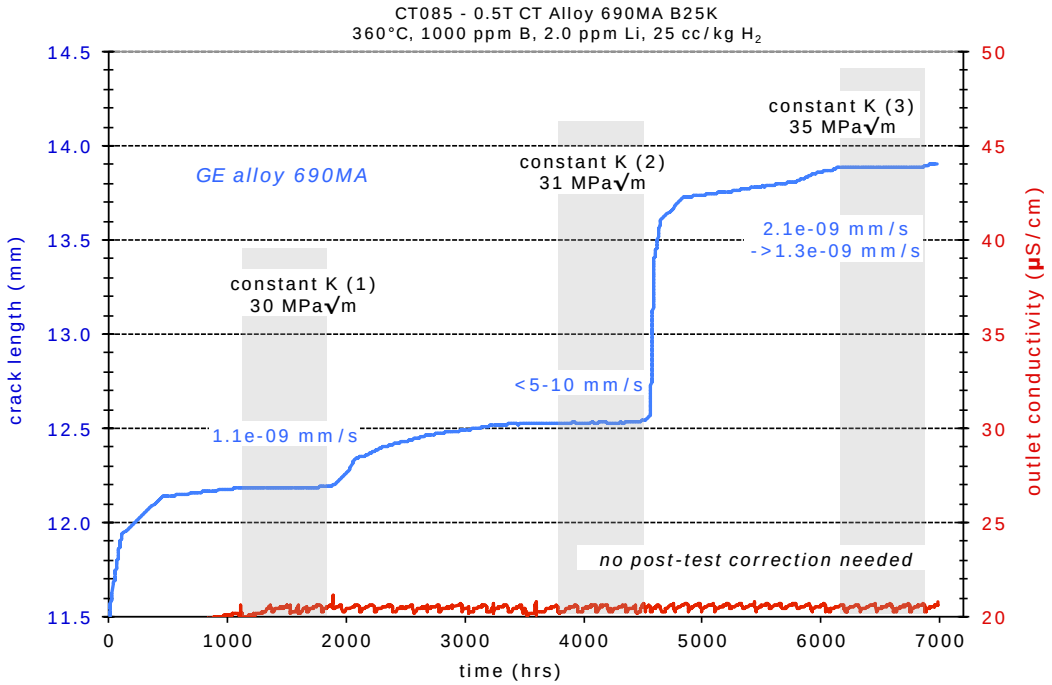


Figure 3. Overview of the entire SCC test on the as-received GEG alloy 690MA specimen CT085.

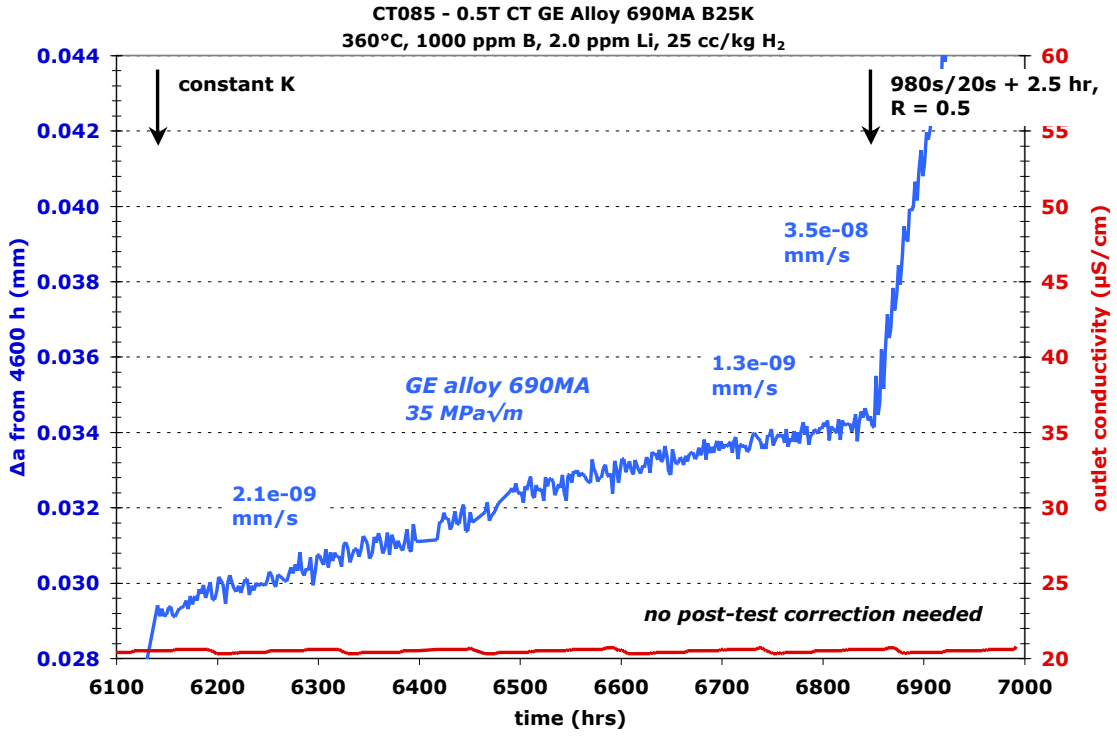


Figure 4. Crack growth response for the as-received GEG alloy 690MA specimen CT085 during the final constant K observation at 35 MPa√m.

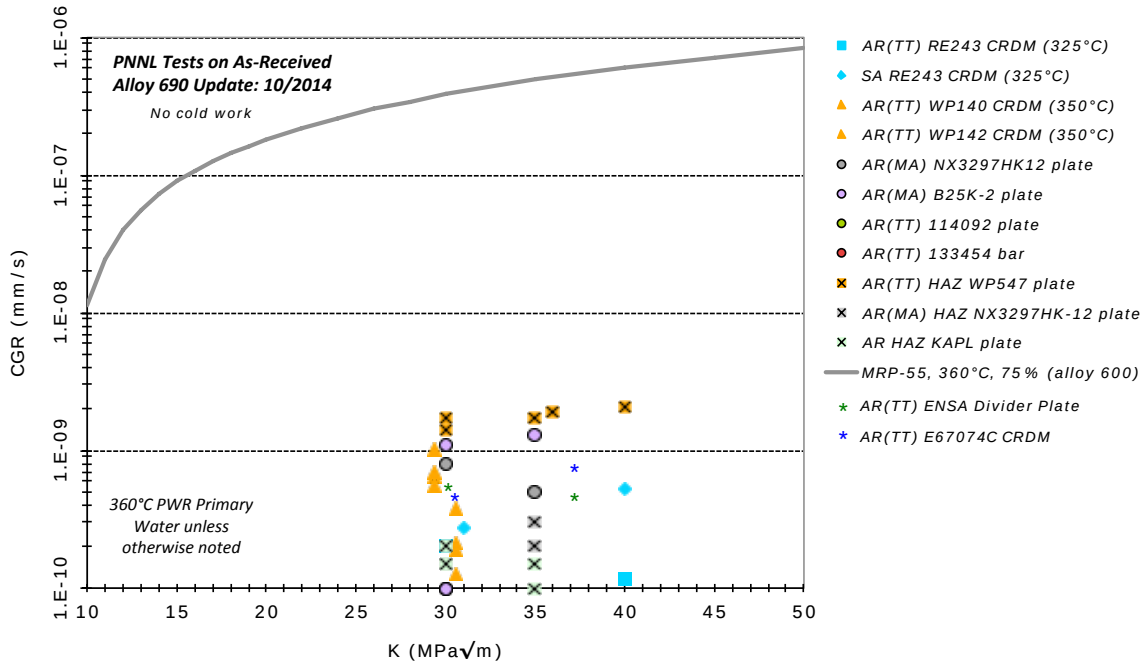


Figure 5. Summary of measured SCC growth rates for alloy 690 CRDM and plate materials without applied cold work. As-received TT and MA materials are included along with a CRDM in the HTA condition and three specimens assessing response for alloy 690 HAZ specimens.

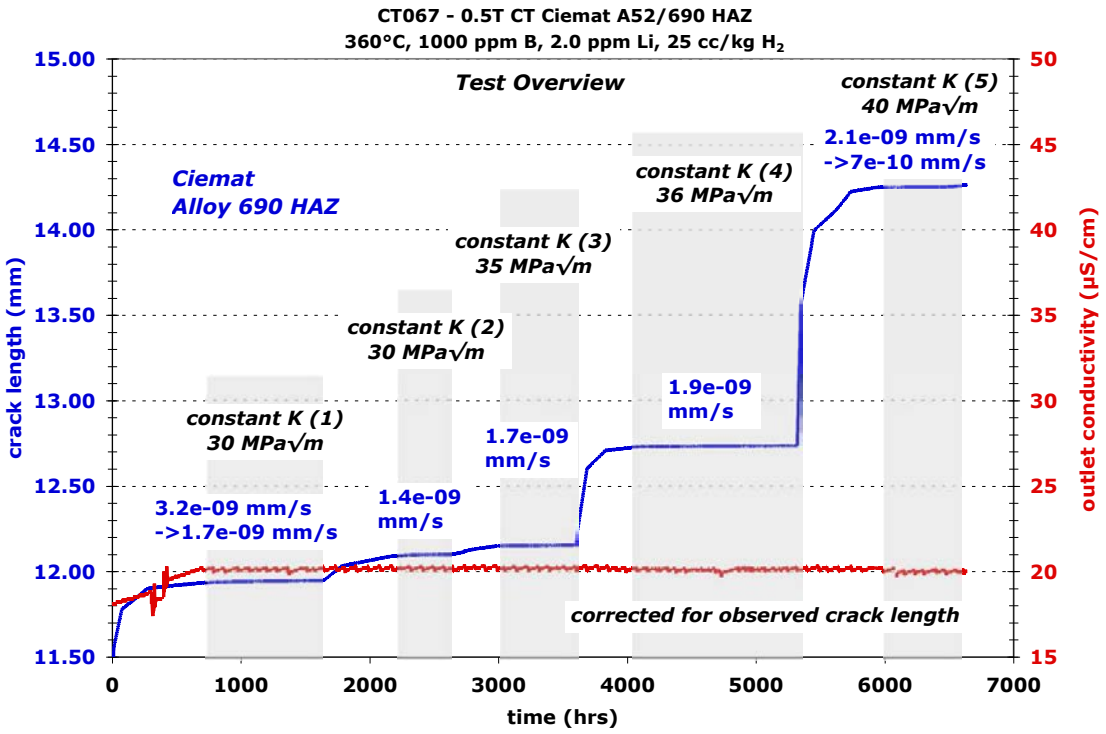


Figure 6. Overview of the entire SCC test on the CIEMAT WP547 alloy 690TT HAZ specimen CT067.

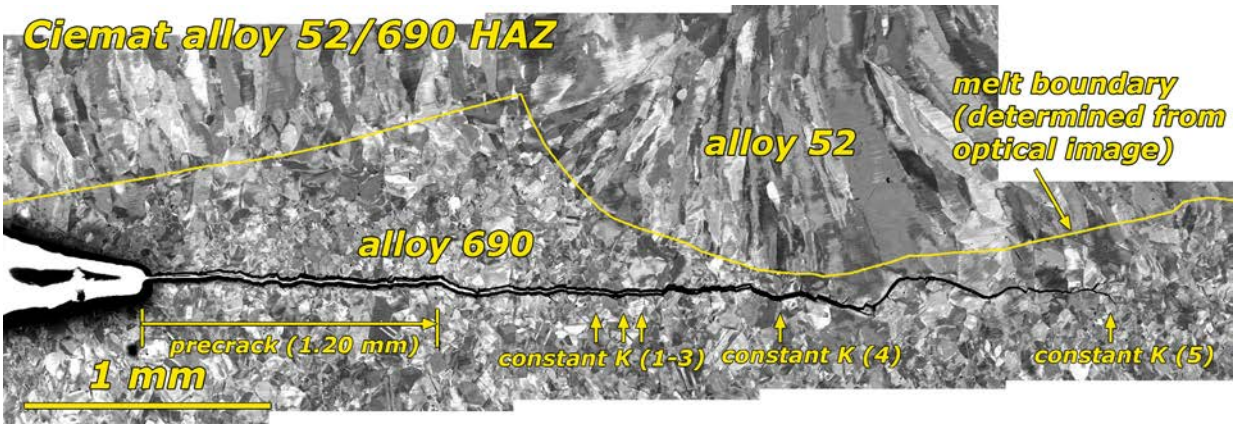


Figure 7. SEM-BSE side surface image of the Ciemat WP547 alloy 690TT HAZ specimen CT067 showing where the constant K measurement in Figure 6 were performed.

**Alloy 690 Materials with Low-to-Moderate Levels of Cold Work**

This represents the cold-work regime where more research is clearly needed to better establish heat-to-heat behavior, particularly since the original data from Bettis [1,2] presented in Figure 1 highlighted a 12%CR plate heat where high SCC growth rates were observed. Since the typical level of cold or warm work in alloy 690 service components and welds is expected to be low, establishing SCC response for materials with lower levels of cold work is critical from a practical point of view for realistic PWR service conditions. Six CRDM specimens have been tested with cold work levels from 11.6-17% with four in the TT condition and two in in the HTA condition. Without question, cold work levels of ~12% can promote IGSCC susceptibility. The most extensively evaluated CRDM heat (RE243) exhibited consistently higher SCC growth rates in the 11.6%CF condition (Figure 8) than for the as-received TT

material. SCC propagation rates were still low at ~4x10$^{-9}$ mm/s for K values of 30 MPa√m, but increased to ~9x10$^{-9}$ mm/s at 42 MPa√m where IG engagement increased to ~50%. Two tests were conducted on 17%CR RE243 material with maximum SCC rates measured at less that ~3x10$^{-9}$ mm/s and limited IG cracking, similar to the response measured for the HAZ specimens. Summary data available in this cold work range are added to results discussed in the prior section and presented in Figure 9. SCC growth rates remain below 1x10$^{-8}$ mm/s for all specimens evaluated.

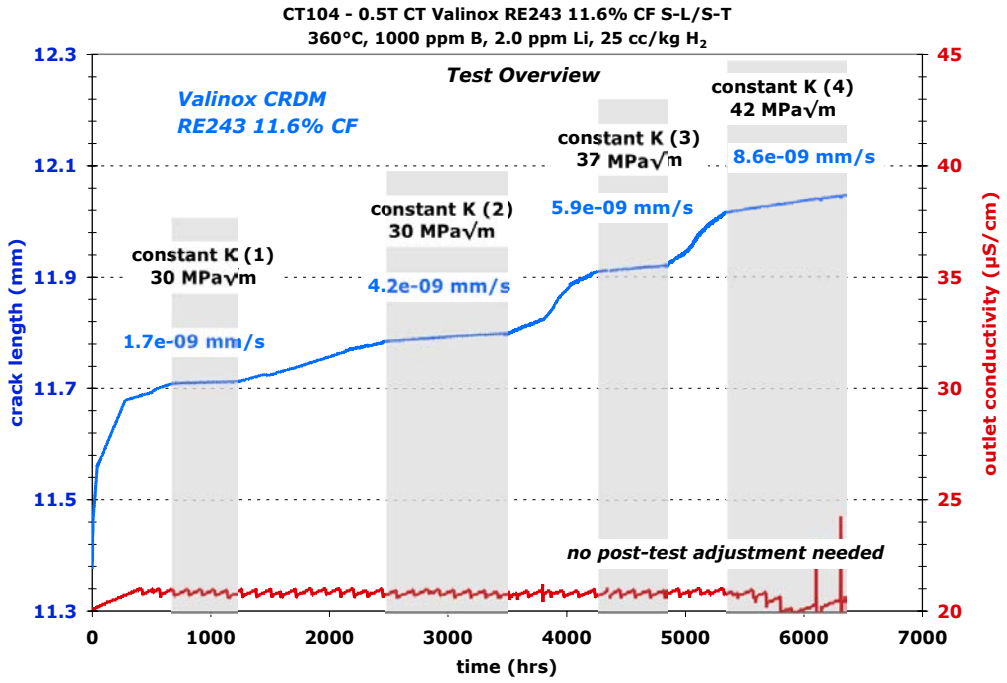


Figure 8. Overview of the entire SCC test on the 11.6%CF CRDM RE243 alloy 690TT specimen CT104.

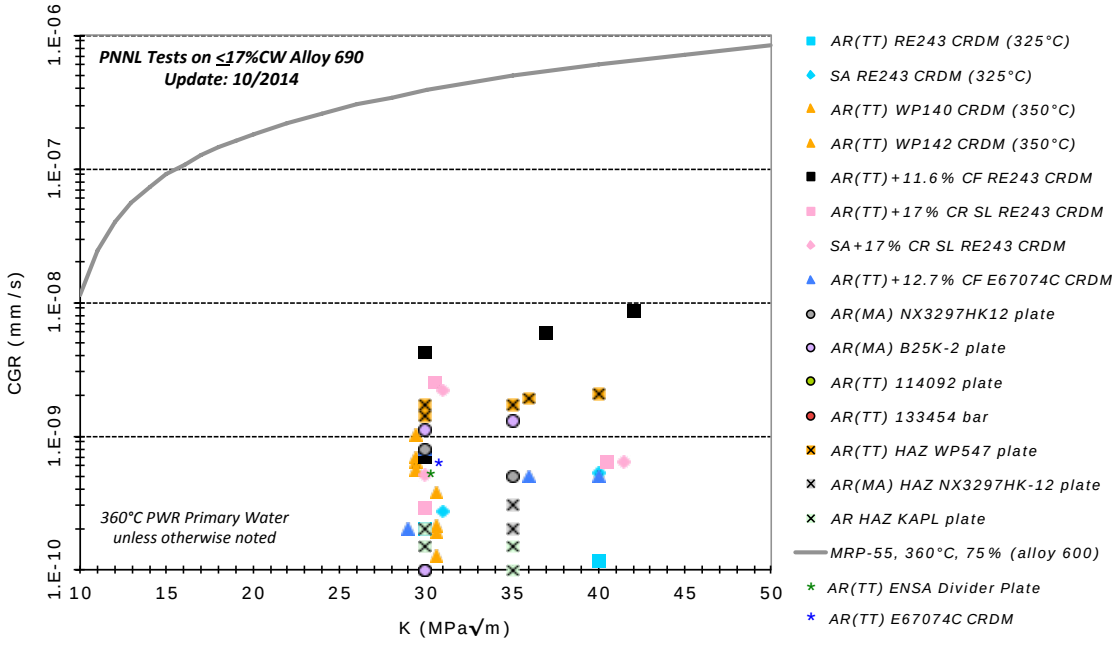


Figure 9. Summary of measured SCC growth rates for alloy 690 CRDM and plate materials with cold work from 0 to 17% reduction.

Existing results suggest that cold work below 17% is not sufficient to promote significant IGSCC susceptibility in the CRDM heats evaluated. Unfortunately, the minimum cold work level evaluated for plate and billet materials has been 20% and will be discussed in the following section. Additional experiments are clearly needed at lower cold work for both CRDM and plate heats.

**Alloy 690 Materials with Moderate-to-High Levels of Cold Work**

The next group of alloy 690 materials examined is six heats cold worked in a narrow range between 20 and 22%. These include an equal number of CRDM and plate/billet heats that have been tested with individual specimens documented in Table 1. As for other cold-work levels, the most extensive testing was on a CRDM heat 243 specimen (CT100) with results shown in Figure 10. Five separate SCC growth rate evaluations were performed at three different K values. Consistent SCC response was observed with measured propagation rates of 2-5x$10^{-8}$ mm/s indicating no significant effect of increasing K from 30 to 43 MPa√m. Reasonably similar SCC growth rates were found for nearly all of the 20-22% cold-worked alloy 690 heats as shown in Figure 11. Only the 21%CF Allvac billet heat (X87N-1) specimen CT101 exhibited propagation rates below 1x$10^{-8}$ mm/s. No obvious reason for this lower SCC susceptibility was discovered, since the TT microstructure and hardness value was comparable to the other TT heats in this group. It is interesting to note that similar SCC growth rates have been measured elsewhere for the 20%CR GE Allvac B25K [6,11] and the 22%CR ENSA SP547 [12] materials, while the 20%TS CRDM WP787 heat exhibited somewhat lower propagation rates in tests at CIEMAT [13]. The promising results from the heats evaluated at this moderate-to-high level of cold work support the inherent SCC resistance of the high Cr, alloy 690 materials. None of the six heats investigated indicated the high SCC susceptibility shown for the 12%CR and 24%CR plate heats by Bettis [1,2] in Figure 1, but some heat-to-heat variability was clearly identified. However, additional alloy 690 heats should be considered particularly materials with inhomogeneous microstructures that may have been put into PWR service.

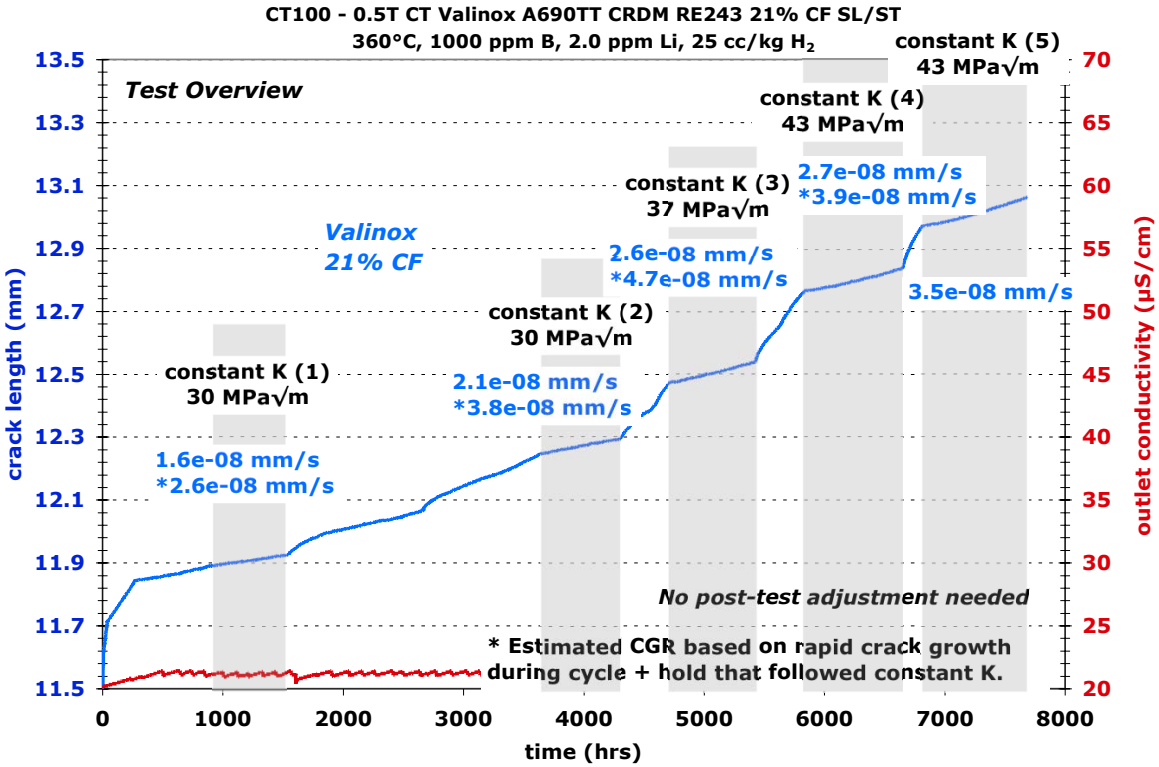


Figure 10. Overview of the entire SCC test on the 21%CF CRDM RE243 alloy 690TT specimen CT100.

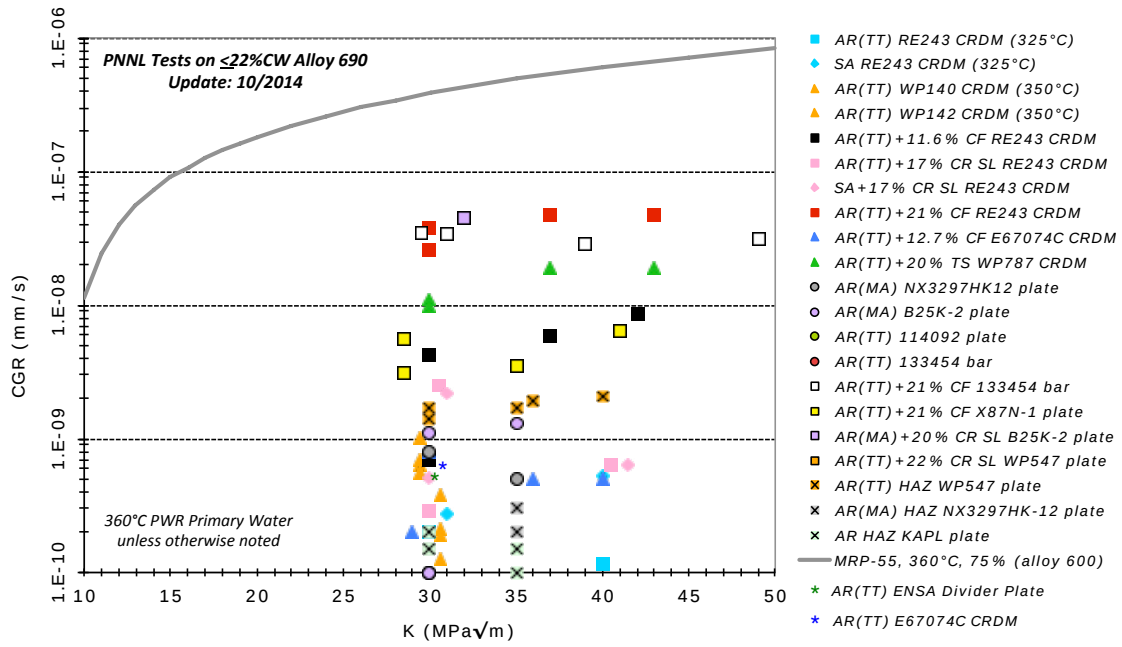


Figure 11. Summary of measured SCC growth rates for alloy 690 CRDM and plate materials with cold work from 0 to 22% reduction.

**Alloy 690 Materials with High Levels of Cold Work**

The last sequence of alloy 690 materials investigated was cold worked from 26-32%, well beyond the maximum strain damage expected for PWR service components except for steam generator plugs. Two as-received CRDM and three plate heats were tested in seven cold-worked conditions. The 31%CF Valinox heat RE243 and Sumitomo heat E67074C exhibited nearly identical SCC growth response at K levels ranging from ~18.5 to 32 MPa√m. Measurements are presented for the Sumitomo specimen CT098 in Figure 12 where SCC propagation rates dropped from ~$2x10^{-7}$ mm/s at 29 MPa√m to ~$2x10^{-9}$ mm/s at 19 MPa√m indicating a threshold-type behavior as K is decreased to low values. A similar crack-growth rate dependence on K is documented for the 31%CF CRDM RE243 specimen CT099 in Figure 13 along with data for five additional highly cold-worked TT and MA materials.

Several of these highly cold-worked materials have been tested elsewhere including the 26%CR ANL plate heat by three laboratories [7,10,11]. Somewhat surprisingly, results have suggested that there may be significant SCC variability depending on location within the plate. Measured SCC growth rates for specimens from one location were 5-10X greater (up to ~$5x10^{-7}$ mm/s) than the other location. Banding and microstructural inhomogeneity has been documented in the plate [16,18], however it has not been directly linked to the observed SCC differences. Contrary to these results, excellent agreement [12,17] has been found during multi-laboratory testing of the 31%CR CRDM RE243 and 32%CF ENSA SP547 materials.

As illustrated in Figure 13, SCC growth rates at K levels of 30-43 MPa√m were between 0.7-$2x10^{-7}$ mm/s for all heats completing the consistent increase in SCC susceptibility with the level of cold work. This relationship is further demonstrated by examining measured crack growth rates at a K of 30-32 MPa√m in Figure 14(a). The red dashed lines in the plot indicate the response for the CRDM RE243 material where a full range of cold work levels was assessed. Only two specimen results fall slightly outside the band, those for the 20%CR GE B25K plate and 21%CF Allvac X87N-1 billet materials. The data suggests a possible change in SCC response with increasing cold work as the level exceeds ~15%.

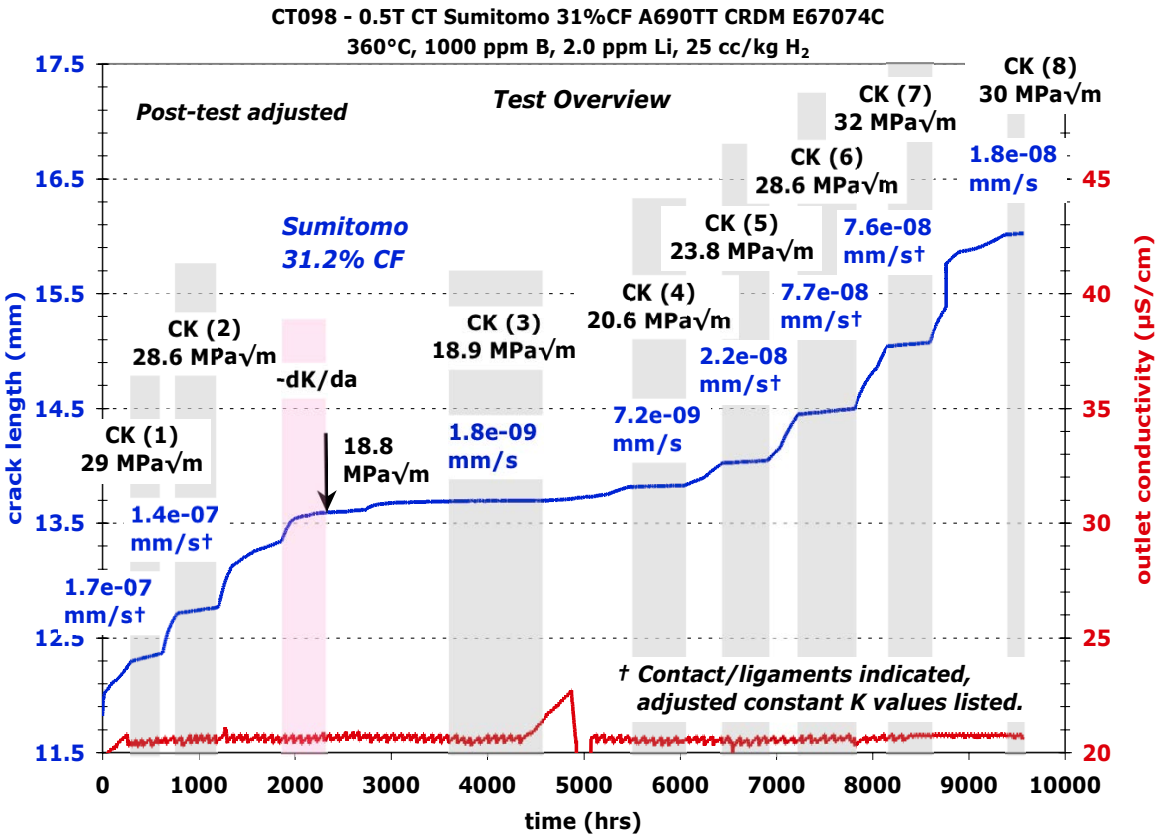


Figure 12. Overview of the entire SCC test on the 31%CF Sumitomo CRDM alloy 690TT (heat E67074C) specimen CT098. Measured constant K (CK) crack growth rates are identified.

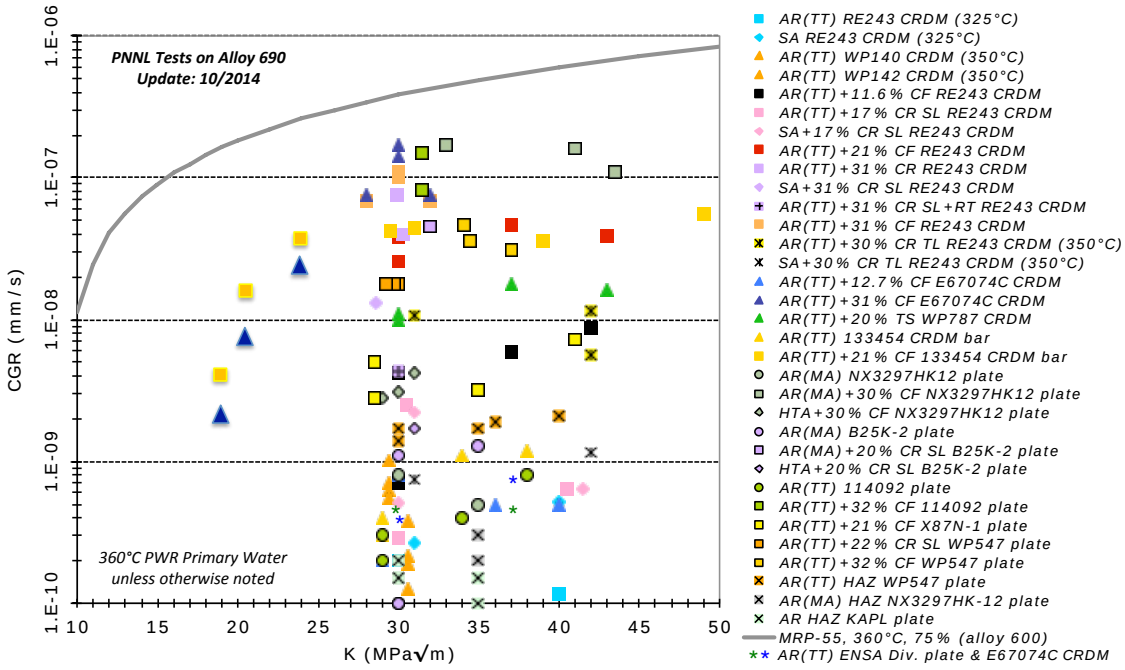


Figure 13. Summary of measured SCC growth rates for alloy 690 CRDM and plate materials with cold work from 0 to 32% reduction.

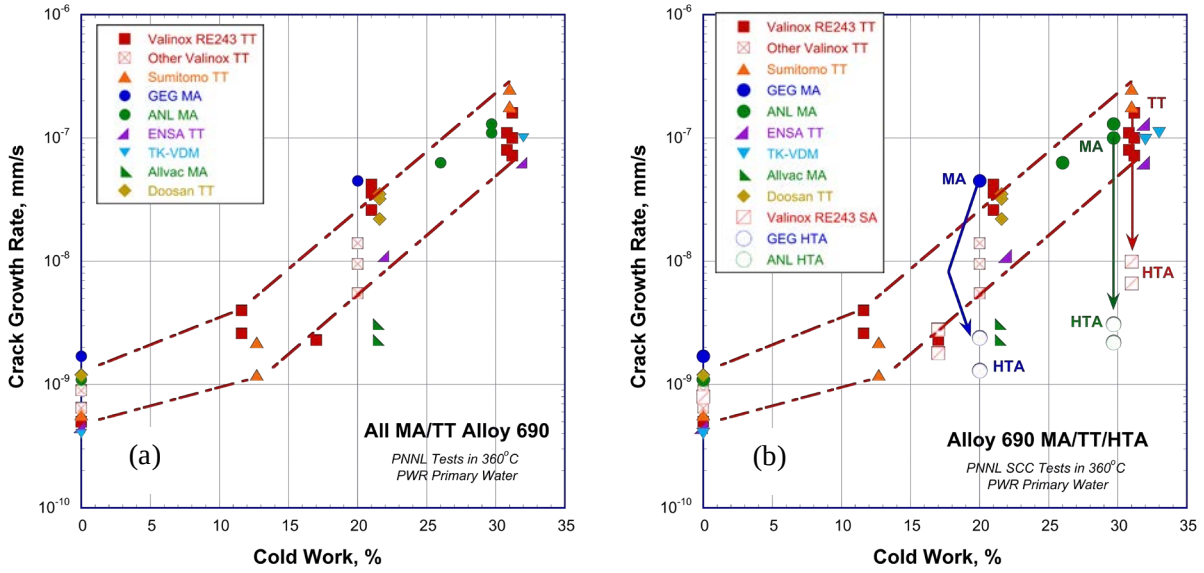


Figure 14. Cold work effects on measured SCC growth rates at a K of 30-32 MPa√m for alloy 690 materials in the as-received MA or TT starting condition (a) and with the addition of HTA materials (b).

**Initial High Temperature Anneal on SCC Susceptibility of Cold-Worked Alloy 690 Materials**

All alloy 690 materials discussed so far started in their as-received, MA or TT condition. In order to gain insights into microstructural effects on SCC susceptibility, three materials were given a HTA treatment as described earlier with microstructural changes summarized in Table 2. Direct comparisons of SCC behavior were then made between identically cold worked materials (31%CR RE243 CRDM, 30%CF ANL plate and 20%CR GE plate). Experimental results for these specimens were described in detail previously [21,22] and revealed SCC growth rates 10-20X lower for HTA materials as illustrated in Figure 14(b). It is also obvious from this plot that propagation rates for the highly cold-worked HTA materials are consistently below the data summary for the as-received, MA or TT materials. Two other RE243 CRDM materials in HTA condition were tested without cold work and cold rolled to 17%, these specimens exhibited the same SCC susceptibility as those in the as-received TT condition.

## HARDNESS AND RESIDUAL STRAIN CORRELATIONS WITH SCC GROWTH RATES

Hardness and EBSD misorientation (residual strain) mapping has been performed on the alloy 690 specimens listed in Table 1 where SCC growth rates in simulated PWR primary water were summarized in the previous sections. Initial comparisons between average hardness and EBSD IMD residual strain values have been presented elsewhere [21-23] for our cold-worked alloy 690 materials. Both hardness and EBSD IMD were shown to increase in a reasonably linear fashion with the % cold work for most materials. Updated correlations to SCC growth rates are presented in Figure 15 with a best-fit dashed line for the CRDM RE243 materials. While hardness and EBSD residual strain measurements do improve correlations to SCC response for specific materials, overall a similar scatter exists among all cold-worked specimens. Once again, the three materials given the initial HTA treatment (31%CR RE243 CRDM, 30%CF ANL plate and 20%CR GE plate) show much lower crack-growth rates than expected based on hardness or residual strain. Even though hardness and IMD values are reduced for the 20%CR GE plate specimen in the HTA condition, neither measurement can reconcile the reduced SCC susceptibility for the cold-worked alloy 690 HTA specimens. In addition, the 21%CF Allvac X87N-1 billet specimen exhibits lower propagation rates as does the 12%CF Sumitomo CRDM specimen. Although it is clear that matrix strain and strength promotes SCC, another aspect must play an important role influencing susceptibility among various materials.

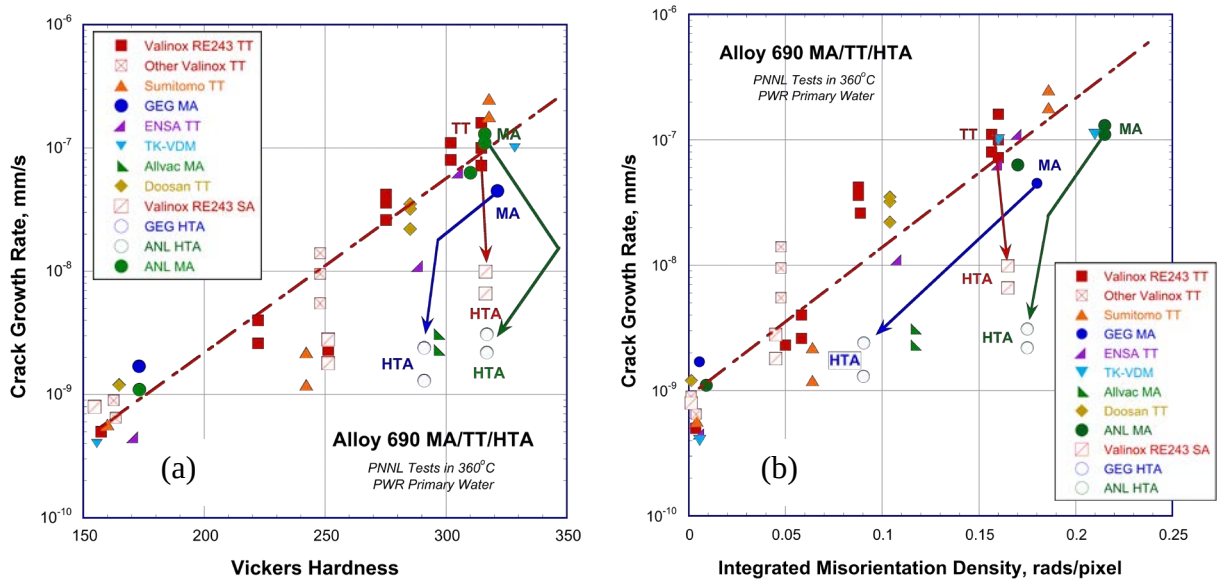


Figure 15. Correlations between hardness (a) and IMD (b) versus measured SCC growth rates for the full range of alloy 690 CRDM, plate and billet materials. Differences in response for the as-received MA and TT materials versus the HTA materials are highlighted.

## COLD WORK EFFECTS ON IGSCC SUSCEPTIBILITY OF ALLOY 690

A systematic evaluation of SCC growth behavior in PWR primary water has been completed on alloy 690 materials as a function of cold work. Six CRDM and six plate/billet heats were tested with cold-work levels ranging from 0 to 32% reduction. While additional experiments on materials with low levels of cold work would be beneficial, the results clearly show a continuous increase in SCC susceptibility with cold work. Low strength alloy 690 without cold work is resistant to IGSCC with measured crack growth rates below ~$2x10^{-9}$ mm/s. Relatively low levels of cold work (~12%) are seen to promote IG cracking in PWR primary water, although SCC growth rates remained below ~$5x10^{-9}$ mm/s for the CRDM heats examined. This SCC response was generally similar to that observed for three alloy 690 weld HAZ specimens where some degree of warm work was present based on hardness measurements. As cold work is increased to ~20%, IGSCC susceptibility is much higher and propagation rates can reach ~$5x10^{-8}$ mm/s for certain heats. Finally, extreme levels of cold work (~30%) promote very high SCC growth rates of $1x10^{-7}$ mm/s or more. In general, these results are in good agreement with SCC measurements from other laboratories [5-15] suggesting that moderate-to-high levels of cold work (greater than ~17%) are required to promote IGSCC susceptibility of concern for alloy 690 materials. The early Bettis data [1,2] on a 12%CR alloy 690 plate shown in Figure 1 remains an exception and may indicate important heat-to-heat or material condition issues that have not yet been identified.

Hardness and EBSD residual strain measurements elucidate the influence of cold work on the matrix strength and dislocation density, respectively. Cold work (>~17%) that promotes significant IGSCC in as-received MA/TT materials corresponds to a hardness greater than ~250 kg/mm$^2$ and an IMD value greater than ~0.07 rads/pixel. Although these values do indicate the transition to materials showing higher IGSCC growth in the current tests, they do not represent thresholds since a continuous increase in SCC susceptibility was observed as a function of cold work, hardness and residual strain. It is interesting to note that hardness measurements were recently reported [2] for several of the Bettis alloy 690 plate materials in Figure 1. Average Vickers hardness numbers of 233-240 and 270-274 were indicated for the 12%CR and 24%CR alloy 690 plate materials with engagement corrected SCC growth rates at a K of ~30 MPa$\sqrt{m}$ of 0.2-$1x10^{-7}$ mm/s and 4-$8x10^{-7}$ mm/s, respectively. The hardness values are generally consistent

with alloy 690 materials in the current study, but SCC measurements are 5-20X above the SCC versus hardness correlation in Figure 15(a). Therefore, strength levels do not explain the enhanced SCC response for the Bettis materials and again points to other heat-to-heat or material condition issues.

The improved SCC resistance of the highly cold-worked alloy 690 HTA materials in the current experiments highlights the critical importance of the initial microstructural condition. Hardness measurements revealed nearly identical strength for the 31%CR CRDM and 30%CF ANL plate materials regardless of starting condition, a small decrease in hardness was seen for the 20%CR GE plate in the HTA versus MA condition. EBSD residual strain distributions did indicate a more significant difference between the HTA and MA conditions for the plate materials, but gave a similar response for the CRDM heat. The primary microstructural changes created by the HTA treatment were the removal of most chromium carbides from grain boundaries and an increase in overall grain size. Very fine $M_{23}C_6$ precipitates were discovered at some boundaries in the GE and ANL HTA materials along with a lower density distribution of smaller carbides in the GE HTA matrix. As discussed in previous papers [20-22], it seems most likely that the change in grain boundary characteristics due to the HTA treatment directly influences local strain distributions during cold working and alters IGSCC susceptibility in highly cold-worked alloy 690. Previous high-resolution examinations [20,21] of alloy 690 microstructures and IGSCC cracks have also revealed that the permanent damage (grain boundary cracked carbides and voids) induced by cold work does not directly promote IGSCC. The primary interaction between these pre-existing features and the IGSCC cracks was crack blunting and not an acceleration of environment-induced growth. The presence of IG carbides was shown to enhance localized grain boundary deformation during cold work and local strains/stresses at interfaces may promote IGSCC susceptibility.

## SUMMARY AND CONCLUSIONS

The influence of cold work on the SCC susceptibility of alloy 690 CRDM and plate materials in PWR primary water has been assessed. SCC growth rates are shown to increase continuously with cold work from 0 to 32% reduction. Detailed characterizations were conducted on all materials including grain structures, matrix and grain boundary precipitates, local damage due to cold work, hardness and residual strain densities. Correlations demonstrated that matrix hardening plays an important role in promoting IGSCC susceptibility, but it does not explain the influence of initial material condition or certain heat-to-heat differences. Hardness and EBSD misorientation density measurements provide a better assessment of SCC susceptibility than the % cold work, however neither measurement properly predicts behavior for all materials. This systematic study on twelve alloy 690 heats supports the conclusion that a high level of cold work (>~17%) is required to produce significant IGSCC susceptibility. However, additional research remains warranted on materials cold (and warm) worked to service-relevant strain levels and build confidence to establish that heat-to-heat and material condition variations will not lead to SCC.

## ACKNOWLEDGEMENTS

Primary support for this research is from the Office of Nuclear Regulatory Research, U.S. Nuclear Regulatory Commission (NRC). The views expressed in this paper are not necessarily those of the NRC. In addition, key support for this work was also obtained from Rolls Royce for EBSD characterizations and the Office of Basic Energy Sciences, U.S. Department of Energy for high-resolution grain boundary examinations. Helpful interactions with G. Oberson and P. L. Andresen are acknowledged along with the technical assistance of R. J. Seffens and C. E. Chamberlin. Pacific Northwest National Laboratory is operated for the U.S. Department of Energy by Battelle Memorial Institute under Contract DE-AC06-76RLO 1830.

## REFERENCES


1. D. J. Paraventi and W. C. Moshier, "Alloy 690 SCC Growth Rate Testing," *Workshop on Cold Work in Iron- and Nickel-Base Alloys,* Ed. R.W. Staehle and J. Gorman, EPRI, Palo Alto, CA, June 2007. Also *Proc. EPRI Alloy 690 Workshop,* EPRI, Palo Alto, CA, October 2007.

2. D. J. Paraventi and W. C. Moshier, "Primary Water Stress Corrosion Growth in Cold Worked Alloy 690 Plate," *Proc. 16th Int. Conf. Environmental Degradation of Materials in Nuclear Power Systems - Water Reactors,"* NACE International, 2014, Paper 9.

3. H. Xu, S. Fyfitch, P. Scott, M. Foucault, R. Killian and M. Winters, *Materials Reliability Program: Resistance to Primary Water Stress Corrosion Cracking of Alloys 690, 52 and 152 in Pressurized Water Reactors (MRP-111),* EPRI, Palo Alto, CA: 2004, 1009801.

4. J. Hickling, *Materials Reliability Program: Resistance to Primary Water Stress Corrosion Cracking of Alloys 690 in Pressurized Water Reactors (MRP-258),* EPRI, Palo Alto, CA: 2009, 1019086.

5. P. L. Andresen, M. M. Morra, J. Hickling, A. Ahluwalia and J. Wilson, "PWSCC of Alloys 690, 52 and 152," *Proc. 13th Int. Conf. Environmental Degradation of Materials in Nuclear Power Systems - Water Reactors,"* Canadian Nuclear Society, 2007.

6. P. L. Andresen, M. M. Morra, K. S. Ahluwalia and J. Wilson, "Effect of Deformation and Orientation on SCC of Alloy 690," *Proc. 14th Int. Conf. Environmental Degradation of Materials in Nuclear Power Systems - Water Reactors,"* American Nuclear Society, 2009, p. 846.

7. B. Alexandreanu, "The Stress Corrosion Cracking Behavior of Alloys 690 and 152 Weld in a PWR Environment," *ibid 6*, 2009, p. 239.

8. P. L. Andresen, M. M. Morra and K. S. Ahluwalia, "SCC of Alloy 690 and Its Weld Metals," *Proc. Fontevraud 7 Int. Symp. Contribution of Materials Investigation to Improve the Safety and Performance of LWRs,* French Nuclear Energy Society, 2010, Paper A010-T04.

9. K. Arioka, T. Yamada, T. Miyamoto and T. Terachi, "IGSCC Growth Behaviors of Alloy 690 in Hydrogenated High Temperature Water," *ibid 8*, 2010, Paper A007-T04.

10. P. L. Andresen, M. M. Morra and K. S. Ahluwalia, "SCC of Alloy 690 and Its Weld Metals," *Proc. 15th Int. Conf. Environmental Degradation of Materials in Nuclear Power Systems – Water Reactors,"* The Minerals, Metals and Materials Society, 2011, p. 161.

11. D. R. Tice, S. L. Medway, N. Platts and J. W. Stairmand, "Crack Growth Testing on Cold Worked Alloy 690 in Primary Water Environment," *ibid 10,* 2011, p. 71.

12. P. L. Andresen, M. M. Morra and K. S. Ahluwalia, "Effect of Deformation Temperature, Orientation and Carbides on SCC of Alloy 690," *ibid 2*, 2014, Paper 7.

13. G. de Diego, M. del Sol Garcia, D. Gomez-Briceno, J. Lapena and F. Perosanz, "PWSCC of Cold-Worked Alloy 690 CRDM and Weld Metals Alloy 52 and 152," *ibid 2*, 2014, Paper 10.

14. T. Yonezawa, "The Effects of Metallurgical Factors on PWSCC Crack Growth Rate in Simulated PWR Primary Water for TT Alloy 690," *ibid 2,* 2014, Paper 12.

15. K. Arioka, T. Yamada, T. Miyamoto and T. Terachi, "IGSCC Growth of Cold Rolled Alloy 690 in PWR Primary Water," *ibid 2*, 2014, Paper 112.

16. S. M. Bruemmer and M. B. Toloczko, "Pacific Northwest National Laboratory Investigation of Stress Corrosion Cracking in Nickel Base Alloys, Volume 1", NUREG/CR-7103, Vol. 1, ML11277A230 and ML11294A228, U.S. NRC, September 2011.

17. S. M. Bruemmer, M. B. Toloczko and M. J. Olszta, "Pacific Northwest National Laboratory Investigation of Stress Corrosion Cracking in Nickel Base Alloys, Volume 2", NUREG/CR-7103, Vol. 2, ML12114A011, U.S. NRC, April 2012.

18. M. B. Toloczko and S. M. Bruemmer, “Crack Growth Response of Alloy 690 in Simulated PWR Primary Water,” *ibid 6*, 2009, p. 706.

19. M. B. Toloczko and S. M. Bruemmer, “Cold Rolling Effects on Stress Corrosion Crack Growth in Alloy 690 Tubing and Plate Materials,” *ibid 10*, 2011, p. 91.

20. S. M. Bruemmer, M. J. Olszta, M. B. Toloczko and L. Thomas, “High-Resolution Characterization of Grain Boundary Damage and Stress Corrosion Cracks in Cold-Rolled Alloy 690,” *ibid 10*, 2011, p. 301.

21. S. M. Bruemmer, M. J. Olszta, M. B. Toloczko and L. E. Thomas, “Linking Microstructure to Stress Corrosion Cracking of Cold Rolled Alloy 690 in PWR Primary Water,” *Corrosion J*, 69-10 (2013) 953.

22. S. M. Bruemmer, M. J. Olszta, N. J. Overman and M. B. Toloczko, “Microstructural Effects on Stress Corrosion Cracking of Cold-Worked Alloy 690 Tubing and Plate Materials,” *ibid 2*, 2014, Paper 8.

23. N. R. Overman, M. B. Toloczko, M. J. Olszta and S. M. Bruemmer, “Strain Correlations in Alloy 690 Materials Using Electron Backscatter Diffraction and Vickers Hardness,” *Proc. Corrosion 2014*, NACE International, 2014, Paper C2014-4255.

24. M. B. Toloczko, N. R. Overman, M. J. Olszta and S. M. Bruemmer "Pacific Northwest National Laboratory Investigation of Stress Corrosion Cracking in Nickel Base Alloys, Volume 3: Stress Corrosion Cracking of Cold-Worked Alloy 690", NUREG/CR-7103, Vol. 3, U.S. NRC, August 2015.